UMH+ULB, Belgium Feb 28 + Mar 2, 2006

LORENTZ NONINVARIANCE AND NEUTRINO OSCILLATIONS

Frans R. Klinkhamer

Institute for Theoretical Physics

University of Karlsruhe (TH)

Email: frans.klinkhamer@physik.uni-karlsruhe.de

main focus: neutrino oscillations

brief excursion: BEC–BCS crossover

---

[1] F.R. Klinkhamer & G.E. Volovik, JETPL **80**, 389 (2004), cond-mat/0407597.

[2] FRK & GEV, IJMPA **20**, 2795 (2005), hep-th/0403037.

[3] FRK & GEV, JETPL **81**, 551 (2005), hep-ph/0505033.

[4] FRK, JETPL **79**, 451 (2004), hep-ph/0403285.

[5] FRK, IJMPA **21**, 161 (2006) hep-ph/0407200.

[6] FRK, PRD **71**, 113008 (2005), hep-ph/0504274.

[7] FRK, PRD **73**, 057301 (2006), hep-ph/0601116.

1. INTRODUCTION

Motivation for experimentalists (theorists):

Current paradigm for neutrino oscillations from mass differences has mixing angles

$$\underline{\theta}_{21} \approx \underline{\theta}_{32} \approx \pi/4\,, \quad \underline{\theta}_{13} \approx 0\,, \tag{1}$$

with T and CP violation suppressed by factor $\sin\underline{\theta}_{13} \approx 0$.

But, perhaps, one angle need not be small if there are other mechanisms operative?

Here, we discuss a model which, at high energies, can have all mixing angles large, allowing for strong T and CP violation (cf. leptogenesis).

Motivation for theorists (experimentalists):

Lorentz invariance perhaps not a fundamental symmetry but an emergent phenomenon?

Massless (or nearly massless) neutrinos could then provide us with a window to "really new physics."

Here, we discuss an idea based on an analogy with condensed-matter physics [1–3] and a specific type of models [4–7].

2. BEC–BCS CROSSOVER

Ultracold quantum gases of fermionic atoms
(e.g., ^6Li at nano-Kelvin temperatures) with tunable interactions (magnetic-field Feshbach resonances).

BEC–BCS crossover:

For s–wave pairing, BCS–type condensate observed [Regal, Greiner & Jin, PRL 92, 040403 (2004), cond-mat/0401554].

Prediction for p–wave pairing [1]:

quantum phase transition between a vacuum state with fully-gapped fermionic spectrum and vacuum state with topologically protected Fermi points (gap nodes).

Simple illustration of this new type of quantum phase transition:

Bogoliubov–Nambu Hamiltonian for fermionic quasiparticles in the axial state of p–wave pairing:

$$H_{\mathrm{BN}} = \begin{pmatrix} |\mathbf{p}|^2/2m - q & c_\perp\, \mathbf{p}\cdot(\widehat{\mathbf{e}}_1 + i\,\widehat{\mathbf{e}}_2) \\ c_\perp\, \mathbf{p}\cdot(\widehat{\mathbf{e}}_1 - i\,\widehat{\mathbf{e}}_2) & -|\mathbf{p}|^2/2m + q \end{pmatrix}, \quad (2)$$

with m the mass of the fermionic atom, $(\widehat{\mathbf{e}}_1,\, \widehat{\mathbf{e}}_2,\, \widehat{\mathbf{l}})$ an orthonormal triad, $\widehat{\mathbf{l}} \equiv \widehat{\mathbf{e}}_1 \times \widehat{\mathbf{e}}_2$ the direction of the orbital momentum of the pair, $c_\perp$ the maximum transverse speed, and q a parameter which can be controlled by the magnetic field near the Feshbach resonance.

Energy spectrum:

$$E^2(\mathbf{p}) = \left(\frac{|\mathbf{p}|^2}{2m} - q\right)^2 + c_\perp^2\, \left(\mathbf{p}\times\widehat{\mathbf{l}}\right)^2 . \quad (3)$$

BEC regime for $q < 0$, with mass gap.
BCS regime for $q > 0$, with two Fermi points [i.e., points in 3–momentum space at which $E(\mathbf{p}) = 0$] :

$$\mathbf{p}_1 = +p_F\,\widehat{\mathbf{l}}\,, \quad \mathbf{p}_2 = -p_F\,\widehat{\mathbf{l}}\,, \quad (4)$$

for Fermi momentum $p_F \equiv \sqrt{2mq}$.

Quantum phase transition at $q = 0$; see Figs. 1 and 2.

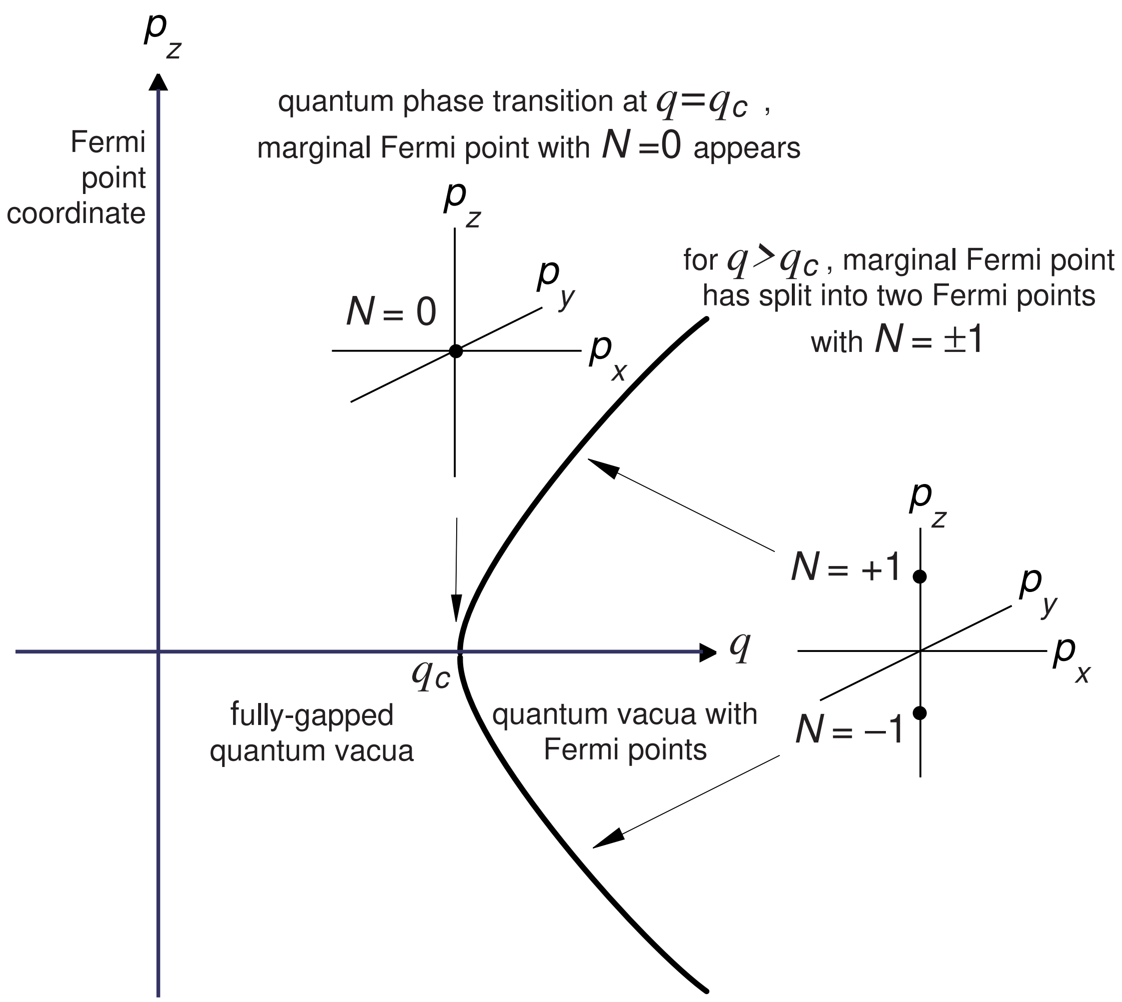

Figure 1: Quantum phase transition at $q = q_c$ between a fully-gapped vacuum and a vacuum with topologically-protected Fermi points (gap nodes). At $q = q_c$, there appears a marginal Fermi point with topological charge $N = 0$ (inset at the top). For $q > q_c$, the marginal Fermi point has split into two Fermi points characterized by nonzero topological invariants $N = \pm 1$ (inset on the right). For a system of ultracold fermionic atoms qualitatively described by Hamiltonian H_{BN}, the critical parameter is $q_c = 0$.

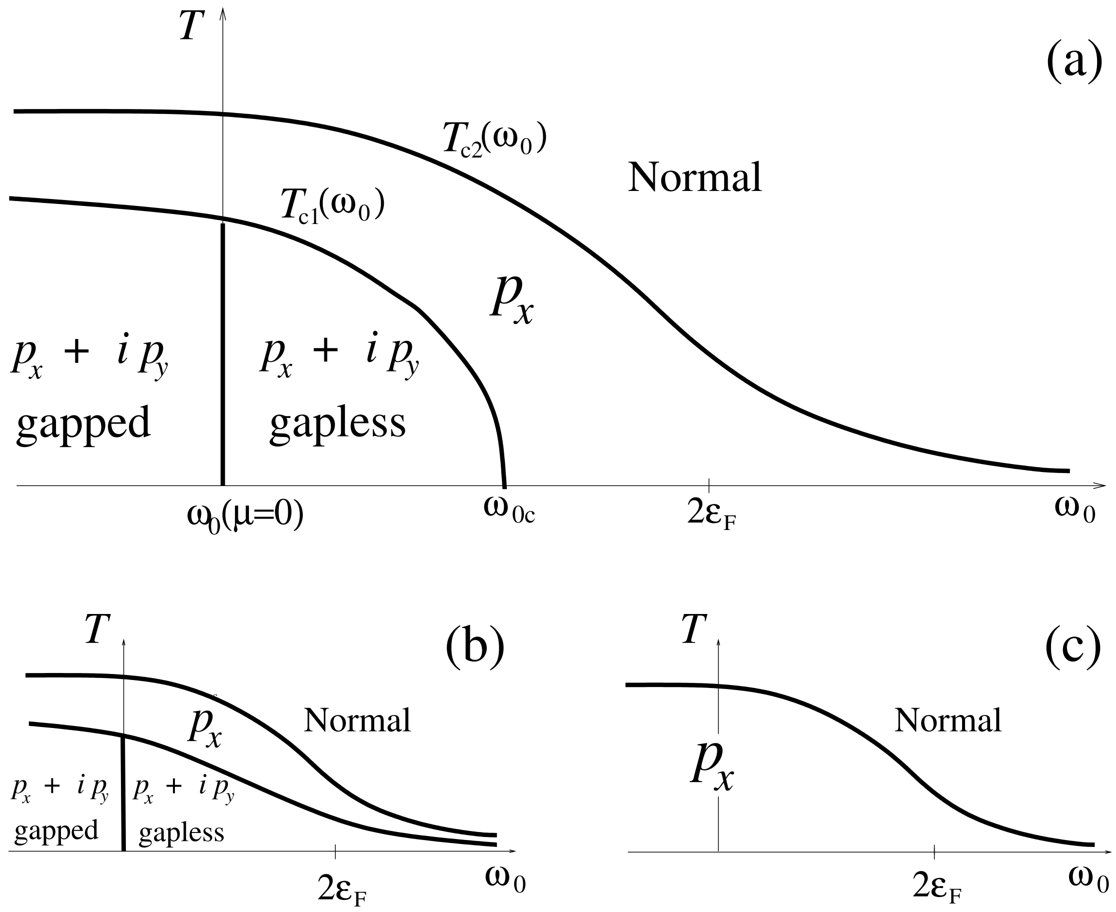

Figure 2: (a): Temperature-detuning phase diagram near a p–wave Feshbach resonance, for intermediate splitting of $m = 0, \pm 1$ Feshbach resonances. Shown are a second-order p_x to $p_x + ip_y$ superfluid transition at ω_{0c} and a topological phase transition at $\mu = 0$ between two different $p_x + ip_y$ phases (quantum critical point at $T = \mu = 0$). (b) and (c): Alternative phase diagrams for smaller and larger values of the Feshbach resonance splitting, respectively. From: Gurarie, Radzihovsky & Andreev, PRL 94, 230403 (2005), cond-mat/0410620.

3. FERMI-POINT-SPLITTING ANSATZ

The chiral fermions of the Standard Model (SM), for vanishing Yukawa couplings, might also have Fermi-point splitting (FPS) in their dispersion laws,

$$\Big(E_{a,f}(\mathbf{p})\Big)^2 \;=\; \Big(c\,|\mathbf{p}| + b_{0a}^{(f)}\Big)^2 \,, \tag{5}$$

where a labels the 16 types of massless left-handed Weyl fermions in the SM (with a hypothetical left-handed antineutrino included) and f labels the fermion families, $f = 1, \ldots, N_F$.

One example of FPS is based on a factorized *Ansatz* [2]:

$$b_{0a}^{(f)} = Y_a \; b_0^{(f)} \,, \tag{6}$$

where Y_a are the SM hypercharge values of the fermions.

For this special pattern, the induced electromagnetic Chern–Simons (CS) term cancels out exactly. (Result is directly related to the absence of perturbative gauge anomalies in the Standard Model.)

This allows for b_0 values larger than the experimental upper limit on the CS energy scale $\approx 10^{-33}$ eV [Caroll, Field & Jackiw, 1990].

Independent of the particular pattern, the dispersion law of a massless left-handed neutrino can be written as

$$\big(E_{\nu_L,f}(\mathbf{p})\big)^2 \;\;=\;\; \Big(c\,|\mathbf{p}| - b_0^{(f)}\Big)^2 . \tag{7}$$

The right-handed antineutrino has

$$\big(E_{\bar{\nu}_R,f}(\mathbf{p})\big)^2 \;\;=\;\; \Big(c\,|\mathbf{p}| - s\,b_0^{(f)}\Big)^2\bigg|_{s=1} . \tag{8}$$

(A value $s = -1$ introduces CPT violation.)

More generally, one may consider for large momentum $|\mathbf{p}|$:

$$E(\mathbf{p}) \;\;\sim\;\; c\,|\mathbf{p}| \pm b_0 + \frac{m^2\,c^4}{2|\mathbf{p}|c} + \mathrm{O}\left(|\mathbf{p}|^{-2}\right) . \tag{9}$$

The energy change from a nonzero b_0 always dominates the effect from mc^2 for large enough $|\mathbf{p}|$.

In order to search for Fermi-point splitting, it is preferable to use neutrino beams with the highest possible energy (or high-energy cosmic neutrinos . . .).

Setting $\hbar = c = 1$, we consider a relatively simple $N_F = 3$ model with both Δb_0 and Δm^2 nonzero.

4. SIMPLE MODEL

For a three-flavor model with both nonzero mass differences and timelike Fermi-point splittings, there are many mixing angles and phases to consider.

The relevant terms of the Hamiltonian in the $(\nu_e, \nu_\mu, \nu_\tau)$ flavor basis are:

$$D_p + X \cdot D_m \cdot X^\dagger + C \cdot Y \cdot D_{b_0} \cdot Y^\dagger \cdot C^\dagger \,, \qquad (10)$$

with diagonal matrices

$$D_p \equiv \text{diag}\,(\,|\mathbf{p}|\,,\,|\mathbf{p}|\,,\,|\mathbf{p}|\,)\,, \qquad (11a)$$

$$D_m \equiv \text{diag}\left(\frac{m_1^2}{2\,|\mathbf{p}|}\,,\,\frac{m_2^2}{2\,|\mathbf{p}|}\,,\,\frac{m_3^2}{2\,|\mathbf{p}|}\right)\,, \qquad (11b)$$

$$D_{b_0} \equiv \text{diag}\left(\,b_0^{(1)}\,,\,b_0^{(2)}\,,\,b_0^{(3)}\,\right)\,, \qquad (11c)$$

and $SU(3)$ matrices given by

$$C \equiv \text{diag}\left(\,e^{i\beta}\,,\,e^{-i(\alpha+\beta)}\,,\,e^{i\alpha}\,\right)\,, \qquad (12a)$$

$$X \equiv M_{32}(\theta_{32}) \cdot M_{13}(\theta_{13}, \delta) \cdot M_{21}(\theta_{21})\,, \qquad (12b)$$

$$Y \equiv M_{32}(\chi_{32}) \cdot M_{13}(\chi_{13}, \omega) \cdot M_{21}(\chi_{21})\,, \qquad (12c)$$

in terms of

$$M_{32}(\vartheta) \equiv \begin{pmatrix} 1 & 0 & 0 \\ 0 & \cos\vartheta & \sin\vartheta \\ 0 & -\sin\vartheta & \cos\vartheta \end{pmatrix}, \tag{13a}$$

$$M_{13}(\vartheta,\varphi) \equiv \begin{pmatrix} \cos\vartheta & 0 & \sin\vartheta\, e^{i\varphi} \\ 0 & 1 & 0 \\ -\sin\vartheta\, e^{-i\varphi} & 0 & \cos\vartheta \end{pmatrix}, \tag{13b}$$

$$M_{21}(\vartheta) \equiv \begin{pmatrix} \cos\vartheta & \sin\vartheta & 0 \\ -\sin\vartheta & \cos\vartheta & 0 \\ 0 & 0 & 1 \end{pmatrix}. \tag{13c}$$

Here, X is the standard MNS mixing matrix.

Further definitions:

$$R_m \equiv \frac{\Delta m^2_{21}}{\Delta m^2_{32}} \equiv \frac{m_2^2 - m_1^2}{m_3^2 - m_2^2}, \tag{14a}$$

$$R \equiv \frac{\Delta b_0^{(21)}}{\Delta b_0^{(32)}} \equiv \frac{b_0^{(2)} - b_0^{(1)}}{b_0^{(3)} - b_0^{(2)}}. \tag{14b}$$

A simple model alright, but a large number of parameters.

Three particular models have been considered in detail:
R (for radical), S (for stealth), and T (for T-violating).

	R–model [4,5]	S–model [6]	T–model [7]	
R_m	0	0	0	
Δm^2_{31}	0	Δm^2	Δm^2	
θ_{21}	–	$\pi/4$	$\pi/4$	bi-max
θ_{32}	–	$\pi/4$	$\pi/4$	bi-max
θ_{13}	–	0	0	bi-max
δ	–	0	0	
R	r	0	1	
$\Delta b_0^{(31)}$	Δb_0	Δb_0	Δb_0	
χ_{21}	$\pi/4$	$\pi/4$	$\pi/4$	tri-max
χ_{32}	$\pi/4$	$\pi/4$	$\pi/4$	tri-max
χ_{13}	$\pi/5$	$\pi/4$	$\pi/4$	tri-max
ω	$-\epsilon$	0	$\pi/4$	
α	–	0	0	
β	–	0	0	

In this talk, we focus on the S– and T–models.

Two remarks on energy scales:

1. Absolute upper bounds from low-energy neutrino physics [Di Grezia *et al.*, hep-ph/0504245] and cosmology:

$$|b_0^{(e)}| \lesssim 1 \text{ keV}\,, \tag{15a}$$

$$\sum_{i=1}^{3} m_i \lesssim 100 \text{ eV}\,, \tag{15b}$$

to which neutrino oscillations can add relative bounds.

2. Emergent-physics scenario [3] with two cutoff scales:

- E_{LV} of fundamental Lorentz-violating fermionic theory,
- E_{c} of compositeness scale of SM gauge bosons.

LEP values of the coupling constants give ($N_F = 3$):

$$E_{\mathsf{c}} \sim 10^{13} \text{ GeV}\,, \quad E_{\mathsf{LV}} \sim 10^{42} \text{ GeV}\,. \tag{16}$$

Perhaps ultrahigh-energy Lorentz violation re-enters at ultralow energy scale:

$$|b_0| \overset{?}{\sim} E_{\mathsf{c}}^2/E_{\mathsf{LV}} \sim 10^{-7} \text{ eV}\,, \tag{17a}$$

which may motivate the search for Fermi-point-splitting effects at the sub–eV level.

5. VACUUM OSCILLATION PROBABILITIES

For large enough neutrino energy E_ν, the vacuum neutrino-oscillation probability from flavor A to flavor B over a travel distance L is readily calculated,

$$P(A \to B, \omega) \;=\; P_{AB}(\,\underbrace{\Delta m^2, \ldots, \beta}_{14 \text{ parameters}}, E_\nu, L\,)\,. \tag{18}$$

The probability for antineutrinos ($s = 1$) is given by

$$P(\bar{A} \to \bar{B}, \omega) \;\;=\;\; P(A \to B, -\omega) \tag{19a}$$

$$\;\;=\;\; P(B \to A, \omega)\,, \tag{19b}$$

which displays CPT invariance.

The time-reversal asymmetry between A–type and B–type neutrinos,

$$\Delta^{(\mathrm{T})}_{AB} \equiv P(B \to A, \omega) - P(A \to B, \omega)\,, \tag{20}$$

is proportional to $\sin\omega$ for the models considered. The corresponding CP discriminant,

$$\Delta^{(\mathrm{CP})}_{AB} \equiv P(\bar{A} \to \bar{B}, \omega) - P(A \to B, \omega)\,, \tag{21}$$

equals (20), for $s = 1$.

6. PHENOMENOLOGY

With both mass differences (MD) and timelike Fermi-point splittings (FPS) present, there are two methods to determine the presence of FPS terms.

The first method is to use sufficiently high neutrino energies E_ν so that the mass-difference effects drop out, $|\Delta m^2/(2E_\nu)| \ll |\Delta b_0|$.

The second method is to look at a particular process which is expected to be small for standard mass-difference neutrino-oscillations. An example is provided by the $\nu_\mu \to \nu_e$ appearance probability at not too large travel distance L,

$$P^{\mathrm{MD}}(\nu_\mu \to \nu_e) \sim \tfrac{1}{2}\,\sin^2(2\theta_{13})\,\sin^2\left(\frac{\Delta m_{31}^2\,L}{4E_\nu}\right), \tag{22}$$

since θ_{13} is known to be small,

$$\sin^2(2\theta_{13})\big|_{\mathrm{CHOOZ}} \leq 0.15\,, \tag{23}$$

at $90\,\%$ CL and $\Delta m_{31}^2 = 2.5\times 10^{-3}$ eV^2.

For high-energy neutrino oscillations over travel distance L, define ($E_\nu \sim |\mathbf{p}|$ and $\hbar = c = 1$):

$$\begin{aligned}
\rho &\equiv \frac{2\,E_\nu}{L\,|\Delta m^2_{31}|} \approx 1.5786 \left(\frac{E_\nu}{10\ \text{GeV}}\right) \\
&\quad \times \left(\frac{10^3\ \text{km}}{L}\right)\left(\frac{2.5\times 10^{-3}\ \text{eV}^2}{|\Delta m^2_{31}|}\right) , \qquad (24a)
\end{aligned}$$

$$\begin{aligned}
\tau &\equiv L\,|\Delta b_0^{(31)}| \approx 5.0671 \left(\frac{L}{10^3\ \text{km}}\right) \\
&\quad \times \left(\frac{|\Delta b_0^{(31)}|}{10^{-12}\ \text{eV}}\right) . \qquad (24b)
\end{aligned}$$

Table 1: $\Delta m^2_{31} = 2.5\times 10^{-3}$ eV^2 ; $\Delta b_0^{(31)} = 1.0\times 10^{-12}$ eV.

experiment	$L\,[\,\text{km}\,]$	$\langle E_\nu\rangle\,[\,\text{GeV}\,]$	ρ	τ
K2K	250	1.0	0.6	1.3
T2K	295	0.7	0.4	1.5
MINOS–ME	735	7.5	1.6	3.7
NOνA	810	2.0	0.4	4.1
ν–factory	1000	10	1.6	5.1

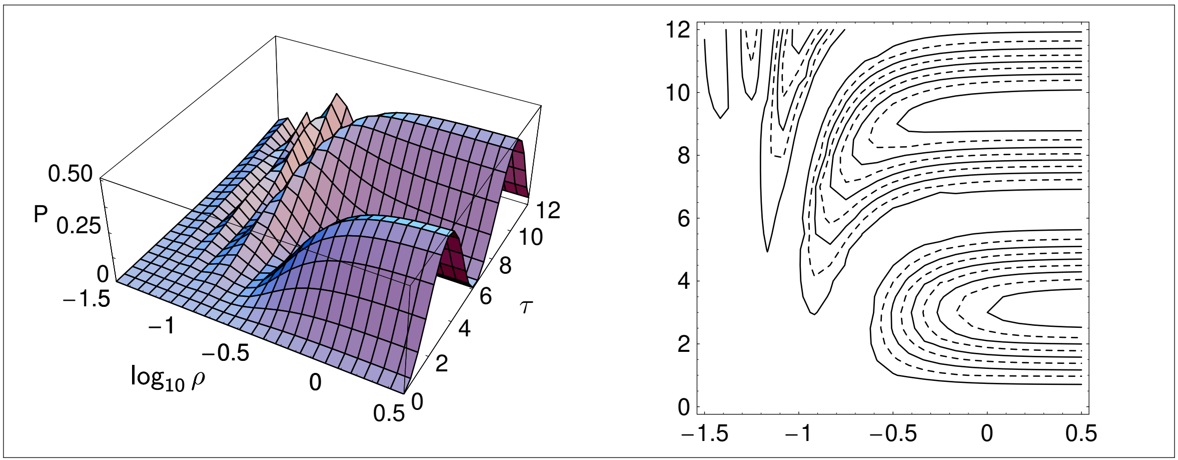

Figure 3: Numerical results for the S–model vacuum probability $P_{\mu e} \equiv P(\nu_\mu \to \nu_e)$. Left: surface plot. Right: contour plot, with equidistant contours at $P_{\mu e} = 0.05, 0.10, \ldots 0.40, 0.45.$

Analytic results (for $R_m = 0$):

- $\lim_{\tau\to 0} P_{\mu e}(\rho, \tau) = 0$

  [pure MD model with $\Delta m^2_{21} = \theta_{13} = 0$];

- $\lim_{\rho\to\infty} P_{\mu e}(\rho, \tau)|_{R=0} = \frac{1}{2}\,\sin^2(\tau/2)$

  [pure FPS model with $\Delta b_0^{(31)} \neq 0$ and trimax mixing];

- for $\rho \to 0$ and fixed τ (arbitrary R and ω),
  $P_{\mu e} \sim (4R^2/S)\,\sin^2[\sqrt{S}\,\tau/(8+8R)]$
  with $S \equiv 4 + 4R + 9R^2$

  [degenerate perturbation theory].

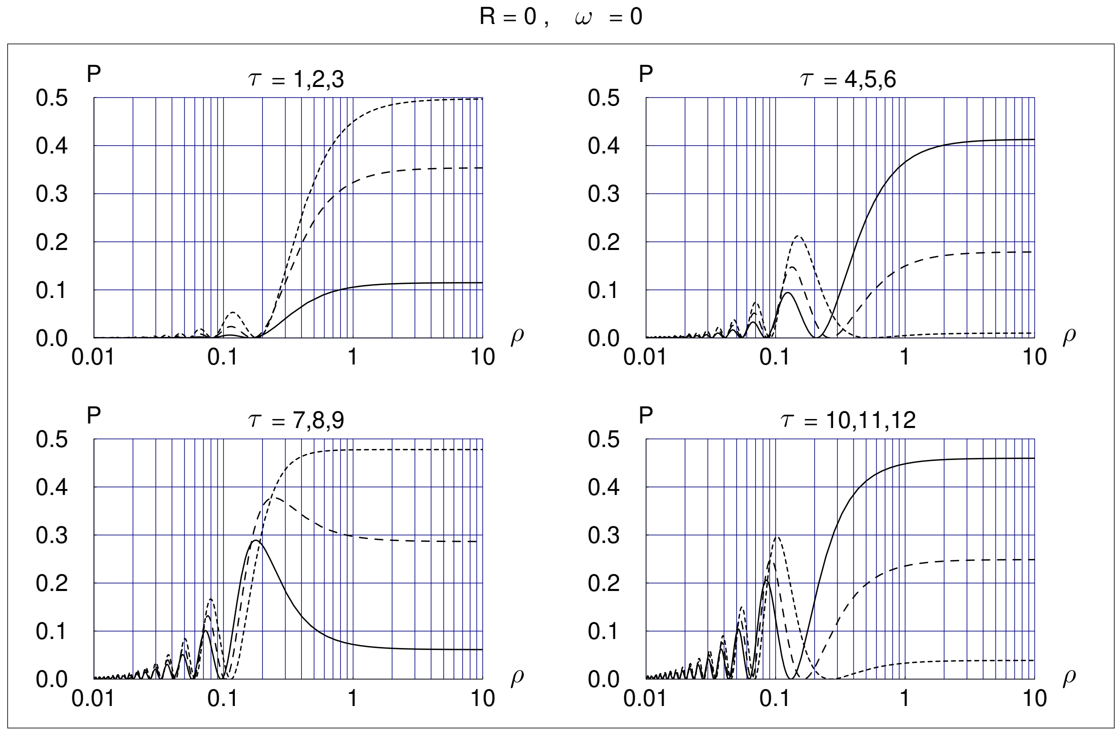

Figure 4: Constant–τ slices of vacuum probability $P \equiv P(\nu_\mu \to \nu_e)$ from Fig. 3. The model has Fermi-point-splitting ratio $R = 0$ and complex phase $\omega = 0$. The curves for positive $\tau = 1, 2, 0 \pmod 3$ are shown as solid, long-dashed, and short-dashed lines.

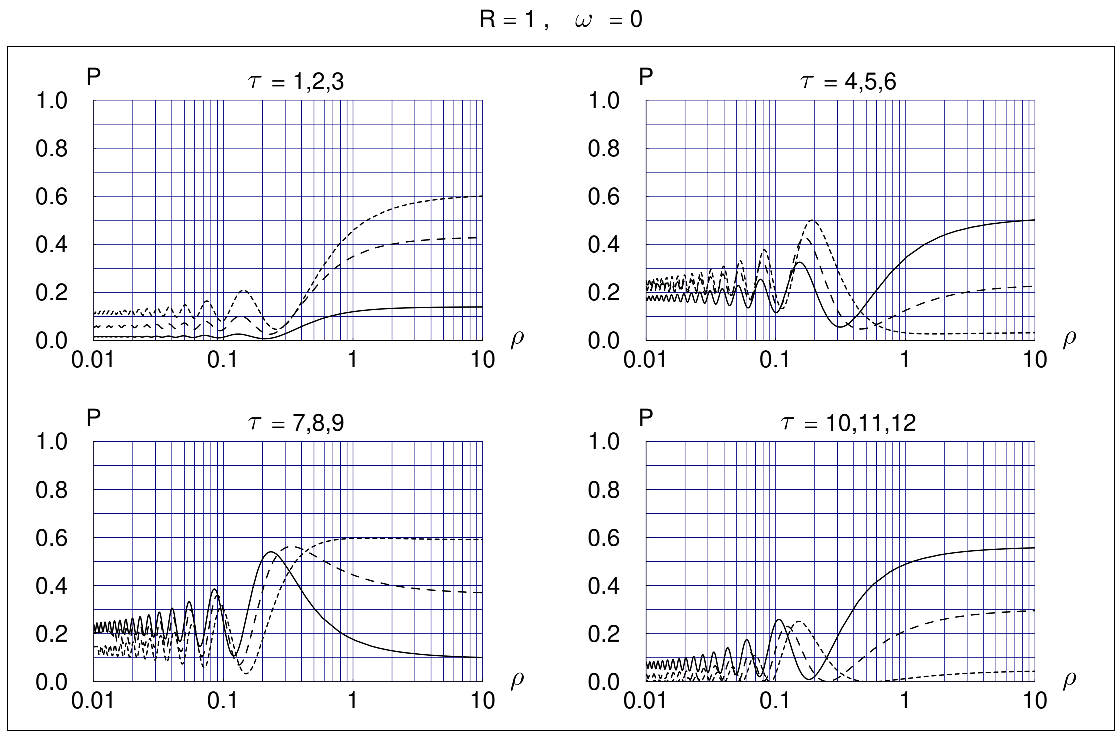

Figure 5: Same as Fig. 4 but for the model with FPS ratio $R = 1$, the complex phase ω still vanishing.

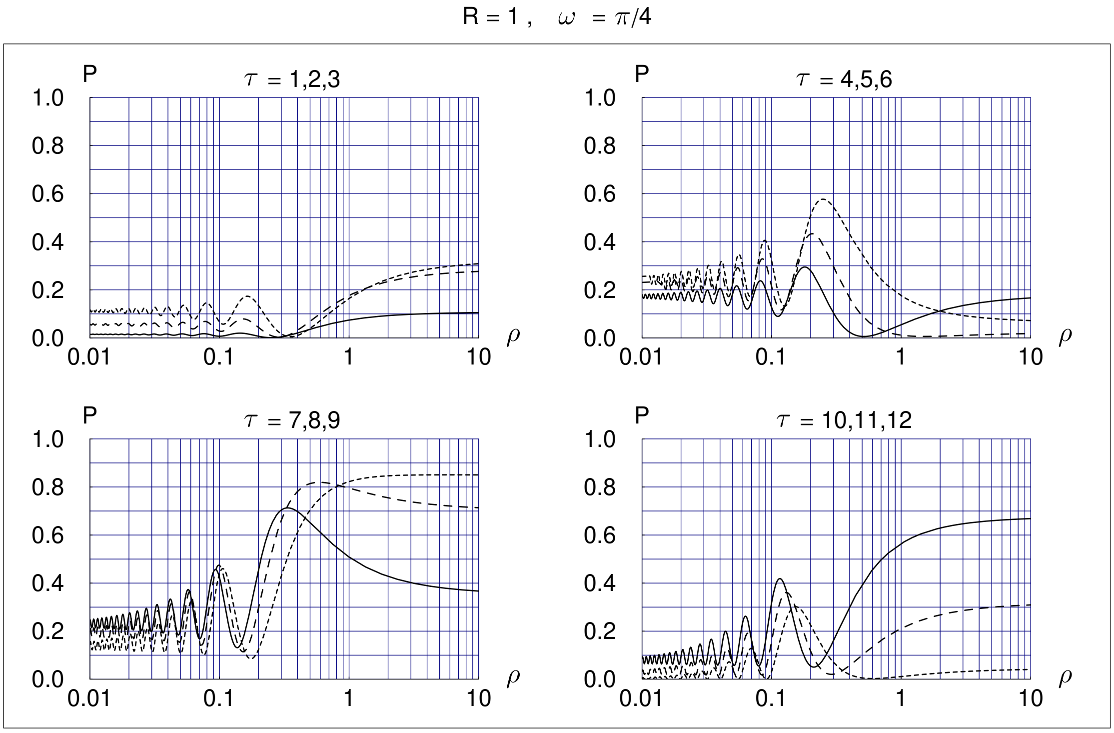

Figure 6: Same as Fig. 5 but now for complex phase $\omega = \pi/4$.

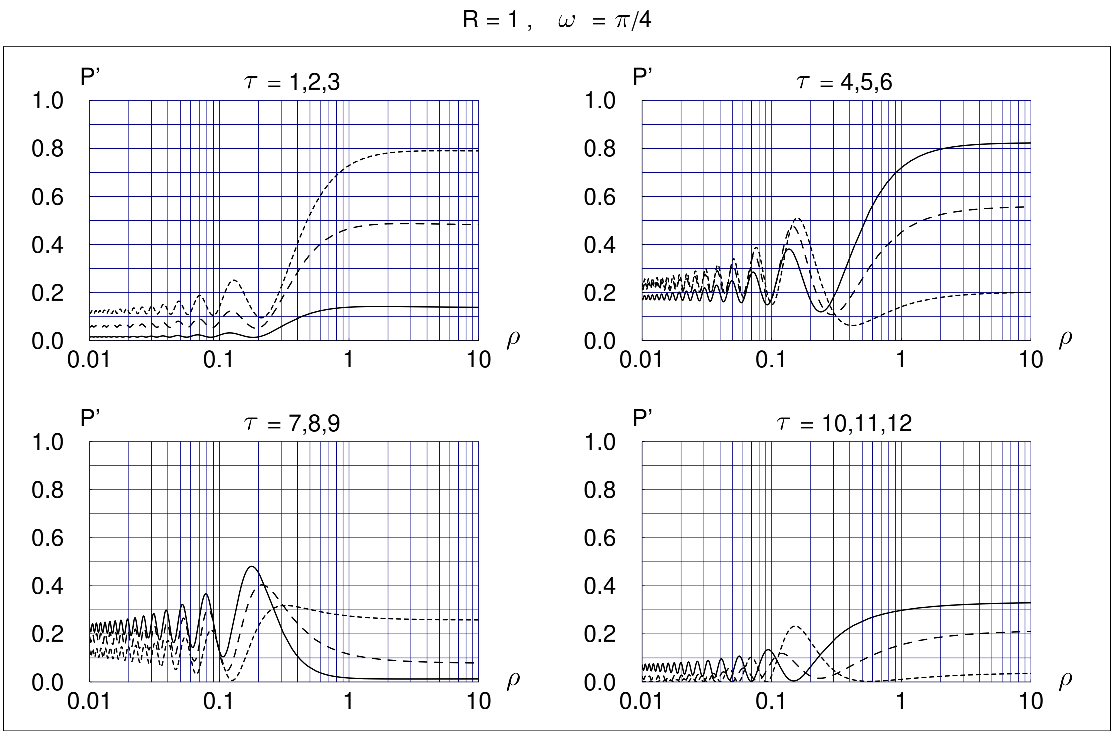

Figure 7: Same as Fig. 6 but for the time-reversed process, with probability $P' \equiv P(\nu_e \to \nu_\mu)$.

$\{R_m, \sin^2(2\theta_{13}), \delta\,;\, R, \sin^2(2\chi_{13}), \omega\} = \{1/30, 1/10, \pi/2\,;\, 1, 1, \pi/4\}$

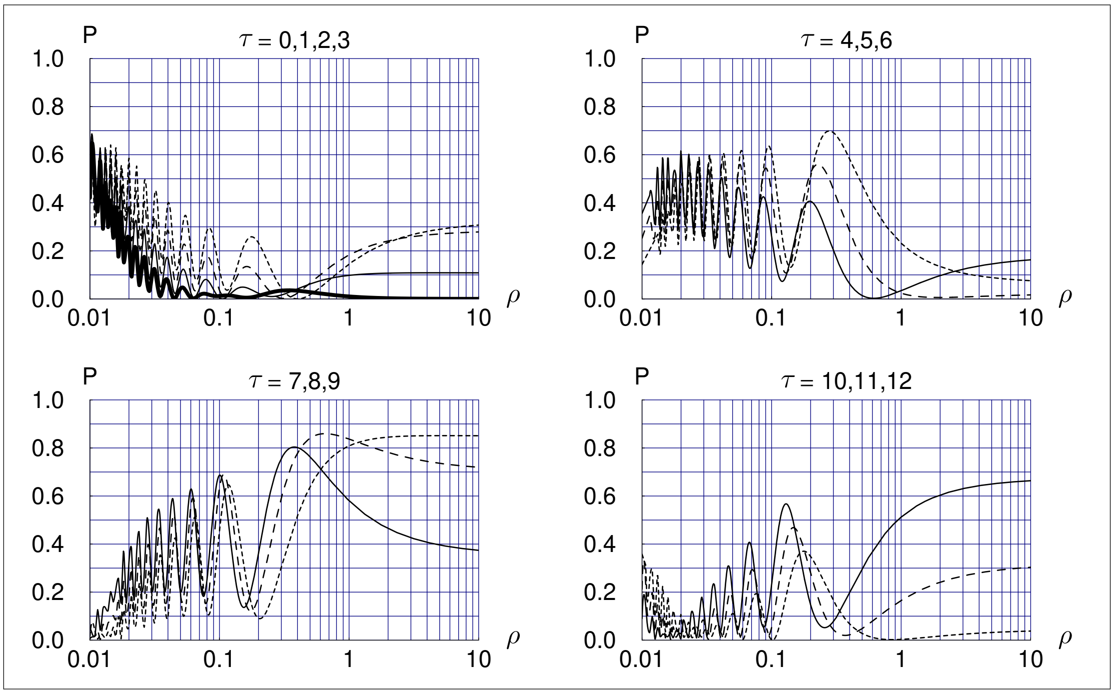

Figure 8: Same as Fig. 6 but now for mass-sector parameters $R_m = 1/30$, $\sin^2(2\theta_{13}) = 1/10$, and $\delta = \pi/2$. The heavy curve in the upper left panel has $\tau = 0$ (pure mass-difference neutrino oscill.).

$\{R_m, \sin^2(2\theta_{13}), \delta\,;\, R, \sin^2(2\chi_{13}), \omega\} = \{1/30, 1/10, \pi/2\,;\, 1, 1, \pi/4\}$

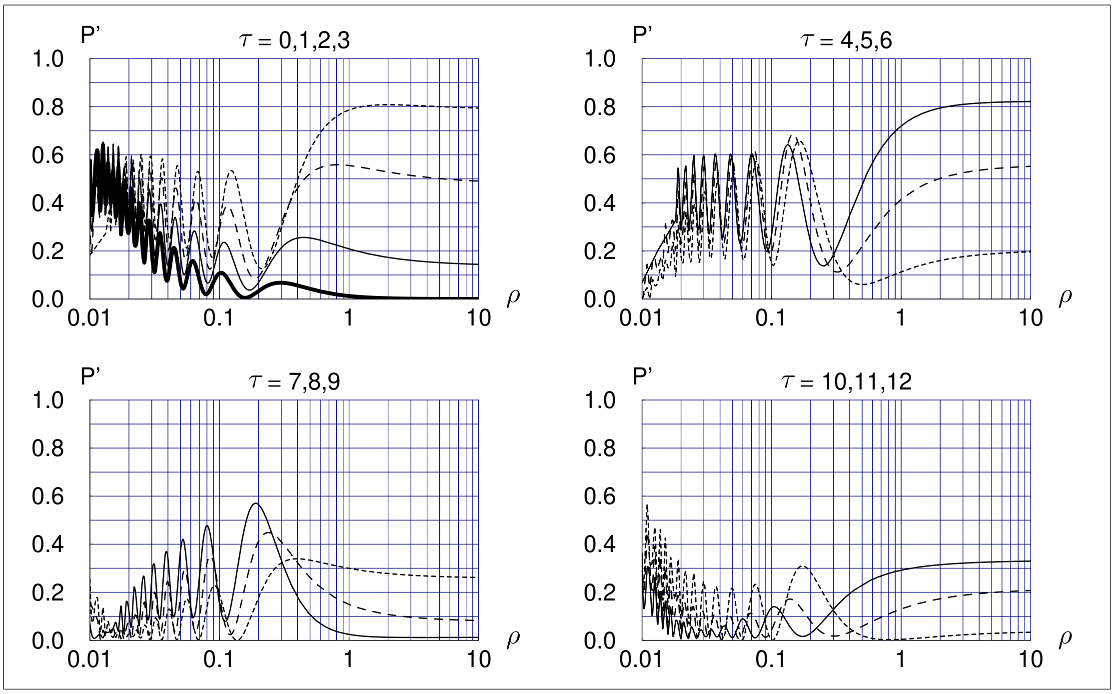

Figure 9: Same as Fig. 8 but for the time-reversed process, with probability $P' \equiv P(\nu_e \to \nu_\mu)$. If CPT invariance holds, P' also corresponds to $P(\overline{\nu}_\mu \to \overline{\nu}_e)$.

7. OUTLOOK

Possible hints of Fermi-point splitting in upcoming neutrino-oscillation experiments:

1. *More or less equal survival probabilities* $P(\nu_\mu \to \nu_\mu)$ *for the medium- and high-energy beam of MINOS?*
2. *Appearance probability* $P(\nu_\mu \to \nu_e)$ *from MINOS–ME/HE (and perhaps ICARUS) above a few percent?*
3. ν_e*–energy spectrum from T2K or NO*ν*A shifted towards higher energy?*

If seen, need to reconsider the future options based on the relevant length scales of the combined mass-difference/Fermi-point-splitting model. And pay special attention to possible strong T–, CP–, CPT–violating effects at the high end of the neutrino energy spectrum.

These future options include superbeams and neutrino factories. [High-energy cosmic neutrinos (AMANDA, IceCube) may also give valuable information.]

But, first, let's see what we can learn from MINOS, ICARUS/OPERA, T2K, . . .